Contents lists available at SciVerse ScienceDirect

Chemical Engineering Research and Design

journal homepage: www.elsevier.com/locate/cherd

Smart RTD for multiphase flow systems

M. Simcik[a], M.C. Ruzicka[a,*], A. Mota[b], J.A. Teixeira[b]

[a] Department of Multiphase Reactors, Institute of Chemical Process Fundamentals, Academy of Sciences of the Czech Republic, Rozvojova 135, 16502 Prague, Czech Republic

[b] IBB-Institute for Biotechnology and Bioengineering, Centre of Biological Engineering, University of Minho, Campus de Gualtar, 4710-057 Braga, Portugal

ABSTRACT

A relatively new concept is presented for evaluation of the fluid age distribution $a = a(\mathbf{x},t)$ within the interior of an apparatus. In the standard RTD approach, the tracer study is performed and the residence time distribution is obtained. In the new approach denoted as SRTD, the fluid age is considered as the field quantity and the governing equation is formulated for its spatio-temporal distribution within the flow domain. There are only few studies devoted to this alternative approach, which typically concern only the single-phase flow systems. In this contribution we investigate its applicability also to multiphase systems. In the case of a bubble column, both the RTD and SRTD concepts are employed and discussed. The results are calculated numerically and compared with the experimental observations.

Keywords: Residence time; Fluid particle age; RTD; SRTD; Multiphase systems; Bubble column

1. Introduction

The tracer concept of RTD (residence/retention time distribution) is the standard part of the engineering education and was developed a long time ago (e.g. Danckwerts 1953, Levenspiel 1962, Froment & Bischoff, 1990, Nauman, 2008). The knowledge of RTD is useful for making a rough picture of the flow pattern inside the equipment, which is usually inaccessible to visual observations. Then, the flow structure can be described with various models dividing the domain into different zones: mixed, piston, shortcuts, dead space, circulation, etc. (e.g. Pareek et al., 2001; Claudel et al., 2003; Rigopoulos & Jones, 2003; Hocine et al., 2008; Montastruc et al., 2009). In case of a flow prevailing in one spatial dimension, like in pipes, the concept of axial dispersion is helpful, and the RTD can be linked to the solution of the 1D convection–diffusion equation, governed by the Peclet number, $Pe = LU/D_{ax}$, where L and U are the length and velocity scales and D_{ax} is the axial dispersion coefficient. The knowledge of RTD is also used for estimation of the conversion in the system, in case of reacting flows. The assumptions typically employed in the RTD are about the closeness/openness of the system, main features of the flow, e.g. flow steadiness, system volume and inflow constancy, etc. Other diffusion-like transport processes may be considered, e.g. gradient molecular tracer diffusion, self-diffusion of fluid molecules, turbulent flow dispersion, etc. The simplest result of the classical RTD experiment is the mean time θ spent by a fluid particle in the system and its variance σ, being the first and second moments of the E-function respectively. The information about the system inside is involved in the I-function.

The RTD is the very first thing to be determined when a chemical engineer approaches an apparatus. We must determine the transfer function of the flow system, i.e. the way how the tracer input (stimulus) is mapped onto the output (response). This information is contained in the record of the exit tracer concentration $c_e(t)$, mass-flow averaged over the exit cross section $\hat{c}_e(t)$. The tracer is assumed to be a 'passive scalar' that sticks to the fluid particle to mark it and to follow the streamlines of the flow field. Usually, an *experiment* with a tracer is performed where the time series of c_e is measured, as a response to the tracer input in the form of a pulse or a step. Several statistical functions based on c_e are used, related to the fluid particles age a, either at the outlet or inside the flow domain. The response $c_e(t)/C_m$ to a *single pulse* is identified with the exit age distribution $E(t)$, where C_m is the mean

* *Corresponding author*. Tel.: +420 220 390 299; fax: +420 220 920 661.
E-mail address: ruzicka@icpf.cas.cz (M.C. Ruzicka).
Received 27 October 2011; Received in revised form 28 February 2012; Accepted 23 March 2012
0263-8762/$ – see front matter © 2012 The Institution of Chemical Engineers. Published by Elsevier B.V. All rights reserved.
http://dx.doi.org/10.1016/j.cherd.2012.03.014

Nomenclature

a	fluid age [s]
c	tracer concentration [mol/m^3]
C_m	mean concentration in the domain (at pulse injection) [mol/m^3]
C_0	inlet tracer concentration [mol/m^3]
d	bubble diameter [m]
D	molecular diffusivity [m^2/s]
D_T	flow dispersivity [m^2/s]
D_{ax}	axial dispersion coefficient [m^2/s]
e	gas volume fraction, gas holdup, voidage, [–]
E	residence time distribution function [s^{-1}]
f	liquid volume fraction [–]
F	residence time cumulative function [–]
g	gravity [m/s^2]
G	internal age cumulative function [–]
h,H	height [m]
I	internal age distribution function [s^{-1}]
k	turbulent kinetic energy [m^2/s^2]
L	length [m]
M	molar mass [mol/m^3]
n	amount of the tracer [mol]; distance in the normal direction [m]
p	pressure [Pa]
r	radial coordinate [m]
Q	fluid input [m^3/s]
q	superficial velocity [m/s]
t	laboratory time [s]
u	gas velocity [m/s]
v	liquid velocity [m/s]
U	mean velocity (gas) [m/s]
V	mean velocity (liquid) [m/s]; volume [m^3]
u'	fluctuating velocity (gas) [m/s]
v'	fluctuating velocity (liquid) [m/s]
$\mathbf{x}$	coordinate vector, (x,y,z) [m]
y	vertical coordinate [m]
Y	mass fraction [–]

Greek letters

ε	turbulent dissipation rate [m^2/s^3]
μ	dynamic viscosity [Pa s]
ν	kinematic viscosity [m^2/s]
κ	bulk viscosity [Pa s]
ρ	fluid density [kg/m^3]
σ	surface tension [N m^{-1}], turbulent Prandtl number [–], second moment of E-function
θ	mean residence time [s]

Subscripts

e	exit/outlet
G	gas
L	liquid
eff	effective
m	mixture
l	laminar
t	turbulent

concentration $\int c_e \cdot dt = n/Q$, where n is the total amount of the tracer injected and Q is volumetric fluid flow rate through the system. The response $c_e(t)/C_0$ to a *single step* is identified with the exit age cumulative function $F(t)$, where C_0 is the input concentration, with the simple relation $E = dF/dt$. Other functions related to the internal age can also be defined, the internal age density distribution $I(t)$ inside the domain, and the internal age cumulative function $G(t)$, where $I = dG/dt$. The following holds, $F + \theta I = 1$, whence $E = -\theta dI/dt$, θ being the mean retention time of the fluid in the system of volume V. The particle age a is often identified with the current laboratory time t, usually set $t = 0$ at the beginning of the tracer experiment. More precisely, one should therefore write $E(a)$, $I(a)$, etc. We thus know the *ensemble distribution* of the particle age a at the exit $E(a)$ and inside the domain $I(a)$. However, we do not know its *spatial distribution* within the domain, $a(\mathbf{x},t)$.

Alternatively, besides the experiment, we can also obtain the exit concentration c_e by the *CFD simulations*, solving numerically the coupled flow and tracer equations. The flow equation, e.g. the incompressible Navier–Stokes equation,

$$\rho\left(\frac{\partial \mathbf{v}}{\partial t}\right) + \rho(\mathbf{v}.\nabla)\mathbf{v} = -\nabla p + \mu\nabla^2\mathbf{v} + \rho g \quad \text{(flow equation)} \qquad (1.1)$$

can be steady or unsteady, according to our assumptions. On the other hand, the tracer equation

$$\left(\frac{\partial c}{\partial t}\right) + (\mathbf{v}.\nabla)c = D\nabla^2 c \quad \text{(RTD tracer equation)} \qquad (1.2)$$

must be unsteady to reflect the tracer evolution within the flow domain. Ideally, the tracer is transported only by convection, to fulfil its marking role truly. Therefore, the unwanted molecular gradient diffusion (D) of the tracer, which always occurs in principle, should be kept to the minimum. The result is the velocity $\mathbf{v}(\mathbf{x})$ or $\mathbf{v}(\mathbf{x},t)$ and concentration $c(\mathbf{x},t)$ fields. The latter is evaluated at the exit from the system to yield c_e(exit, t), whence the exit age distribution functions E and F.

The CFD approach to RTD has been employed for both single-phase and multi-phase flows. In experimental multiphase flows, it can be difficult to separate the different phases from the mixture and analyse them promptly for the tracer content. Also, each phase may need a different tracer, which can pass through the interface. This problem is avoided by using CFD at the price of its weakness to manage the realistic multiphase flows and the uncertainty of the computed results. There are studies published, which follow the CFD approach. For instance, Cockx et al. (1999) performed the Euler–Euler CFD simulations of RTD in ozonation tower plant and obtained good agreement with experimental data. Andreux et al. (2008) studied RTD in a fluidized bed reactor, both experimentally and with CFD. The RTD data were evaluated for the plug flow with axial dispersion. Although vertical pressure profiles were predicted well by the CFD, there were discrepancies regarding the mixing of solid phase. Le Moullec et al. (2008) carried out Euler–Euler simulations of RTD in a cross-flow gas–liquid wastewater treatment reactor and obtained good agreement with experimental data. Ekambara & Joshi (2003) performed Euler–Euler simulations of RTD for a bubble column and found good agreement with experimental data.

The convection–diffusion equation governing the tracer behaviour, Eq. (1.2), can be manipulated in a certain way, to obtain the *spatial distribution* of the *mean age* (locally time averaged), under steady flow condition (e.g. Spalding, 1958, Danckwerts, 1958). We thus have the function $\bar{a}(x)$. This opens a new perspective with large potential (Danckwerts, 1958): "*...a quantitative method of investigating rates of replacement of*

material in various parts of a continuous-flow plant (or of air in a room or water in a pond)...".

As the next step, we are even able to calculate the spatial distribution of the *instantaneous fluid particle age* to obtain $a(\mathbf{x},t)$. To our best knowledge, this approach was pioneered by Sandberg (1981) who introduced this new concept into the area of civil engineering, derived Eqs. (1.3) and (1.4) below, and evaluated the ventilation efficiency in buildings properly. In this concept, the fluid age a is considered as a scalar field variable $a(\mathbf{x},t)$. The quantity a is the actual age of a fluid particle occurring in the time t at the point $\mathbf{x}$ inside the flow domain. Imagine that each fluid particle wears a watch, showing time $t=0$ at the flow domain entrance. Then the particle age a in the time moment t simply is: $a=t$. Thus the age a of a control fluid particle convected by the stream coincides with the current laboratory time t. The motion of such a particle in the Lagrangian frame is described by the total derivative D/Dt. Consequently, the governing equation of the fluid age of any fluid particle is given by

$$\frac{Da}{Dt}=1. \quad \text{(SRTD age equation)} \tag{1.3}$$

It is the advection equation for the scalar variable a, with the source term of strength 1. The source term reflect the fact, that the particle age (a) coincides with the current time (t). The balance of the fluid age in the Eulerian frame for an incompressible flow then reads

$$\left(\frac{\partial a}{\partial t}\right)+(\mathbf{v}.\nabla)a=1, \quad \text{(SRTD age equation)} \tag{1.4}$$

The velocity field $\mathbf{v}$ must be known beforehand or be obtained from a suitable flow equation, e.g. Eq. (1.1). As for the boundary, at the inlet, $a=0$ (when using solvers for 2-nd order PDE, at the walls $\partial a/\partial n=0$ and at the outlet a is extrapolated from the last domain cell).

To distinguish this new approach form the common RTD, we can denote it as SRTD (Smart RTD). The RTD gives only the ensemble distribution of the internal age $I(a)$ for a steady flow. The SRTD gives the space-time distribution of the instantaneous fluid age $a(\mathbf{x},t)$ for a general flow (in steady flow $\partial a/\partial t=0$). With RTD, the diffusion of the tracer in the carrying fluid naturally occurs and is reflected by the D-term in the macroscopic Eq. (1.2), being driven by the concentration gradient. With SRTD, no such process exists, since the particle age does not spontaneously flow from an 'older' particle to a 'younger' particle and therefore no diffusion term appears in Eq. (1.4). However, in case we consider a micro-mixing in the fluid itself, in both Eqs. (1.2) and (1.4) there would be an additional term due to some statistical micro-process (e.g. the self-diffusion of the fluid molecules).

To our best knowledge, there are only very few studies on SRTD in the literature. Davidson and Olsson (1987) did 2D and 3D simulations of room ventilation with several air inlet configurations and obtained fields of local air age in the room. Baléo and Le Cloirec (2000) performed CFD simulations for a single phase flow in an axisymmetric duct with annular obstacles. They solved steady form of Eq. (3.4.1) numerically to obtain field of fluid age and compared radial profiles of fluid age with experimental measured profiles. The simulation results were compared with the experimental data (locally measured age of fluid) and a good agreement was found. Baléo et al. (2001) did a CFD simulation of SRTD in a lagoon pilot using the age equation and compared the results with the tracer experiment where the local residence time was measured in several points. A good agreement was found. Ghirelli and Leckner (2004) presented a theory and model equations for simulation of the local fluid age for single and multicomponent mixtures and for turbulent flow. Ghirelli et al. (2006) did a CFD simulation of a flow in a grate furnace and obtained field of local fluid age inside the furnace. The smart approach to RTD was briefly discussed by Ruzicka (2008). More recently the SRTD was discussed by Liu and Tilton (2010) and Liu (2011). They performed 2D simulations of SRTD for a single phase flow in their test reactor and proposed an elegant way, how to obtain the classical RTD from SRTD simulations, by solving also equations for higher moments of age a distribution. They also discussed in detail differences in possible definitions of fluid age (mean tracer age vs. fluid particle age) and problems associated with solving the fluid age equations. It seems that SRTD has not been used for multiphase flows yet.

The goal of this study is to apply SRTD to a bubble column, as a typical representative of two-phase gas–liquid flow systems. The paper has the following structure. First, to validate the numerical calculations and to establish the correspondence between the standard and new approaches to the retention time distribution, both RTD and SRTD were determined for a model single-phase flow, where the analytical solution is known. Both the tracer equation (Eq. (1.2)) and the fluid age equation (Eq. (1.4)) were solved, together with the flow equation (1.1) (Section 2). Second, both RTD and SRTD was calculated for the liquid phase in a laboratory scale bubble column, solving the tracer equation or the fluid age equation with two-phase Euler–Euler equations for the bubbly mixture (Section 3). Third, the experiments were performed with the tracer technique, to determine the RTD of the liquid phase in the bubble column and the measurements are compared with the simulations (Section 4).

2. Validation of CFD approach for RTD and SRTD

To test the RTD and SRTD calculations, a simple flow situation was considered, Fig. 1a. Here, with the steady laminar flow of a simple liquid between two parallel walls, we have both the analytical and numerical solutions, with a direct physical insight. The two parallel walls have separation $H=10$ cm and length $L=100$ cm (Fig. 1a). The 2D simulation with Fluent v. 12.1 was performed, with the parabolic initial velocity profile and the liquid mean velocity of 1 cm/s. The liquid density and viscosity were that of water, $\rho=1000\,\mathrm{kg/m^3}$ and $\mu=0.001\,\mathrm{kg/m\,s}$. At the outlet, a constant static pressure was set and all other variables were extrapolated from the interior values (pressure-outlet boundary conditions). The no-slip condition was set on the walls. Computational grid had 40×100 cells. The PRESTO! discretization scheme was used for pressure, the QUICK scheme for momentum. The SIMPLE algorithm was used for the pressure–velocity coupling. Time step size was 0.1 s, time discretization was 1-st order implicit.

On the known steady velocity field $\mathbf{v}(x,y)$ calculated by the CFD, the virtual RTD experiment with the tracer was performed numerically. At the inlet, a step change of the tracer concentration was prescribed (from $c=0$ to $c=100$ arbitrary units) and the unsteady tracer equation (Eq. (1.2)) was solved numerically to find $c(x,y;t)$. The exit concentration was mass-flow averaged (i.e. weighted by $\rho_i\cdot v_i$ in the i-the exit cell) over the cross-section area to obtain the response curve $\hat{c}_e(t)$. The

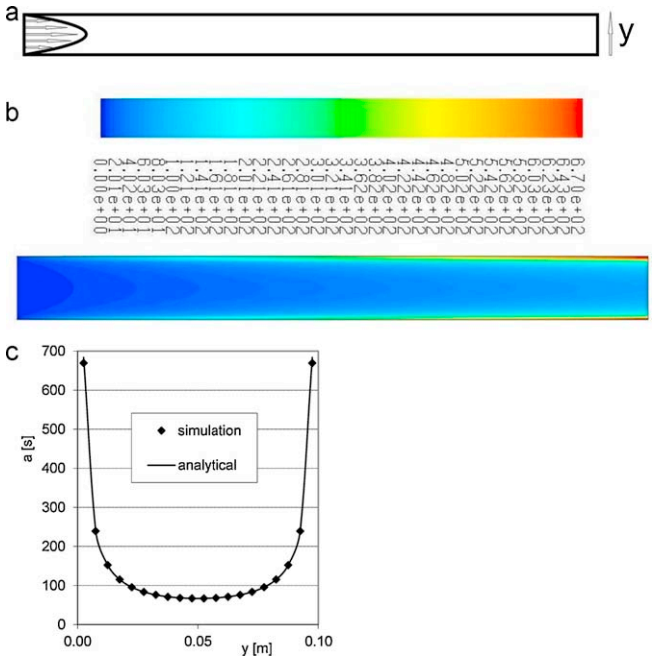

Fig. 1 – Test case for SRTD. (a) Laminar flow between two parallel plates with parabolic profile, plates spacing $H = 10$ cm, length $L = 100$ cm, fluid mean velocity 1 cm/s. (b) Spatial distribution of fluid age $a = a(x,y)$ within the 2D flow domain in steady state computed by CFD. (c) Exit profile of the fluid age $a = a(y)$ at the outlet of the flow domain: CFD simulation vs. analytical result.

cumulative function of the exit age then was $F(t) = \hat{c}_e(t)/C_0$. This *first procedure* is denoted as "F-tracer RTD".

In a similar way, the steady spatial distribution of the fluid age $a(x,y)$ was calculated for the known flow field $\mathbf{v}(x,y)$ by the SRTD approach solving Eq. (1.4). The fluid age increases uniformly along the streamlines, as shown in Fig. 1b. The exit age profile over the cross-section is seen in Fig. 1c. The calculated profile (marks) agrees with the analytical solution (line) given by $a = L/v$, where L is the system length and $v(y)$ the velocity of the respective flow y-lamina. At the wall, the velocity is zero and the age is infinite, thanks to the no-slip boundary condition.

To relate the both approaches, RTD and SRTD, the standard RTD quantities should be obtained from the SRTD data. The standard F-function was calculated from SRTD data in two different ways: from the definition of F and from the definition of I.

For the former way using F, we need the knowledge of the velocity and the fluid age at the exit. The velocity component in the exit cell normal to its face was used, to get

$$F(t) = \left(\frac{1}{Q}\right) \Sigma v \cdot \Delta S \cdot J(t), J(t) = 1 \quad \text{for } a < t, J(t) = 0 \text{ for } t > a,$$

(F-SRTD, way 1) (2.1)

where the sum is over the grid cell faces ΔS at the outlet. This *second procedure* is denoted as "F-SRTD, way 1".

For the latter way using I, we have to evaluate the internal age function I as

$$I(t) = \left(\frac{1}{V}\right) \Sigma \Delta V \cdot K(t),\ K(t) = 1 \quad \text{for } t - \Delta t < a < t,\ K(t) = 0$$

otherwise, (F-SRTD, way 2) (2.2)

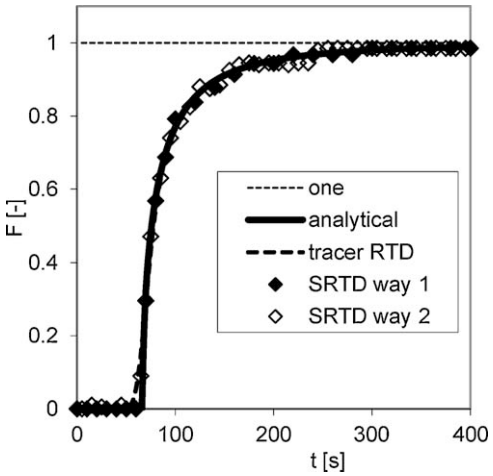

Fig. 2 – RTD cumulative distribution function $F(t)$ of the exit fluid age ($t = a$) obtained by four procedures (see Section 2). First, by the numerical CFD tracer experiment, which is the standard RTD approach. Second, by calculation of F directly from the SRTD numerical data by Eq. (2.1). Third, by calculation of F indirectly from the SRTD numerical data by Eq. (2.2) with help of $I(t)$. Fourth, by analytical solution given by Eq. (2.3).

where the sum is the volume-average that runs over the grid cells ΔV inside the domain, Δt is time discretization interval. Having I, the function F then is: $F(t) = 1 - \theta I(t)$. This *third procedure* is denoted as "F-SRTD, way 2".

The Eqs. (2.1) and (2.2) provide the link between the two approaches, namely how to obtain RTD information from SRTD data. Usually, they need to be solved numerically. In our test case (Fig. 1), they can be solved also analytically. As an example, Eq. (2.1) is solved for F, for the known exit age profile $a(y) = L/v(y)$, with the known exit velocity profile $v(y) = (3/2)U[1 - (y/R)^2]$. $F(a)$ is evaluated as the integral $(1/Q)$ $\int v \cdot dS$ over the exit area S, i.e. from 0 to $y(a)$, where $y(a)$ is the inverse function to $a(y)$. The result is:

$$F(a) = \frac{3}{2}\left(1 - \left(\frac{2}{3}\right)\left(\frac{L}{Ua}\right)\right)^{0.5}\left(1 - \left(\frac{1}{3}\right)\left(1 - \left(\frac{2}{3}\right)\left(\frac{L}{Ua}\right)\right)\right)$$

(F-SRTD analytical) (2.3)

where L is the channel length, U is the mean fluid velocity. This *fourth procedure* is denoted as "F-SRTD, analytical".

The above four different 'procedures' of obtaining the F-function are compared in Fig. 2. The fine steps on the F-curve from the SRTD (way 1) are due to the finite number (40) of the grid cell faces at the discretized outlet boundary. The same tests were performed also for the case of circular geometry, a flow in a pipe, and the results were equally good (not shown). Fig. 2 proves that the RTD and SRTD approaches are compatible. The data of SRTD can be converted or reduced to the data of RTD, since the former approach comprehends a larger amount of information than the latter.

3. Calculation of RTD and SRTD for a bubble column

The 3D flow fields for both the gas and liquid phases of the gas–liquid mixture confined in a bubble column was calculated first. After certain period of time, the quasi-steady flow fields of the gas phase $\mathbf{U}(\mathbf{x})$, the liquid phase $\mathbf{V}(\mathbf{x})$ and the pressure $p(\mathbf{x})$ were obtained. Then the data for both RTD and

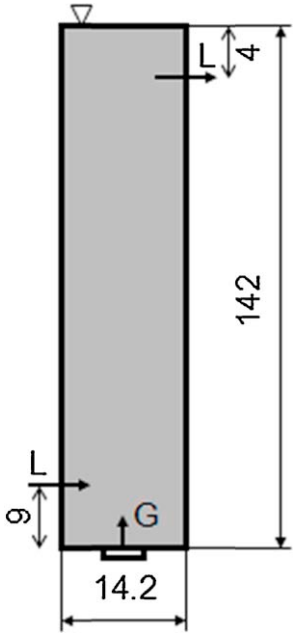

Fig. 3 – Definition sketch of the experimental bubble column that also is the CFD simulation flow domain. Cylinder of diameter $d = 14.2$ cm and height $H = 142$ cm, gas phase G, liquid phase L. The vertical plane of the geometric symmetry passes through the inlet/outlet pipes of G phase.

SRTD were obtained numerically, using the liquid phase velocity field $\mathbf{V}(\mathbf{x})$. For RTD, we calculated the tracer concentration field $c(\mathbf{x},t)$ and evaluated the exit response curve $c_e(t)$. For SRTD, we calculated the spatial distribution of the liquid age $a(\mathbf{x})$.

3.1. *Geometry of simulated bubble column*

The calculations of RTD and SRTD were done for a 3D lab-scale bubble column shown in Fig. 3, which was used also for the tracer RTD experiments described in Section 4. The plexiglas cylindrical column had the inner diameter 0.142 m and the ungassed liquid height 1.42 m (aspect ratio 1:10). Both the gas (air) and liquid (water) phases were fed continuously into the column. The liquid entered the column through the circular inlet orifice 1.6 cm dia, placed in the column wall 8.5 cm above the bottom. The liquid outlet of 6 mm dia was placed at the height of 1.38 m. The gas was distributed by a small perforated plate of 2.5 cm dia, placed 4.5 cm above the bottom of the column. The plate had 30 orifices, each 1 mm dia. The liquid throughflow had two values, $Q_L = 44$ and 80 l/h, which corresponds to the liquid flow rate (superficial velocity $q = Q/S$) $q_L = 0.8$ and 1.4 mm/s. The gas throughflow had three values, $Q_G = 2$, 5, 10 l/min, which corresponds to the gas flow rate $q_G = 2.1$, 5.3 and 10.5 mm/s. These parameter values were chosen in correspondence with the specific kind of our biotechnology applications. The following four combinations were both calculated and measured, denoted as Cases A–D, see Table 1.

3.2. *Calculation of gas–liquid flow in bubble column*

The two interpenetrating continua Euler–Euler approach was used to simulate the gas–liquid flow in our bubble column (e.g. Ranade, 2002; Rafique et al., 2004; Prosperetti and Tryggvason, 2007). The governing equations can be derived by ensemble averaging the fundamental conservation equations for each phase in the multiphase mixture. The flow fields of all the phases are described by the continuity and momentum equations. In our case, there is one set of these equations for the gas phase and one for the liquid phase. These equations are coupled together via the interphase force terms, the volume fraction field, and the single pressure field that is shared by the both phases. The two-phase equations and the technical details are put in Appendix A. The numerical flow solver Fluent 12.1 was used in this study.

Table 1 – Parameter values used for the bubble column for Cases A–D. Liquid and gas flow rates (Q_L, Q_G) and the corresponding superficial velocities (q_L, q_G).

	Q_L [ml/s]	Q_G [ml/s]	q_L [mm/s]	q_G [mm/s]
Case A	12.2	33.3	0.8	2.1
Case B	22.2	33.3	1.4	2.1
Case C	22.2	83.3	1.4	5.3
Case D	22.2	166.7	1.4	10.5

The Cartesian $\mathbf{x} = (x,y,z)$ computational 3D domain was a cylinder 1.42 m high of 0.142 m diameter (Fig. 3). The number of the grid cells was 94,200 and the time step was 0.005 s. To fit the cylindrical shape, the grid cells were deformed cubes of size approximately 5 mm × 10 mm × 5 mm, except near the bottom, where it was finer, 5 mm × 5 mm × 5 mm for $h < 10$ cm.

The gas outlet boundary condition at the top was as follows. The liquid velocity $\mathbf{V}$ was set to zero (no inflow/outflow through the top boundary). The gas velocity $\mathbf{U}$ and the gas holdup e were extrapolated from their interior values (values at grid cell boundary faces set equal to cell centre values). The gas inlet boundary condition had the gas velocity U equal to 25 cm/s, the gas volume fraction was then adjusted to obtained the desired gas flow rate. The liquid inlet and outlet areas were 2 cm × 2 cm squares at heights $h = 8$ and 138 cm, respectively. Gas volume fraction was prescribed to be zero, liquid velocity was set such that the required liquid flow rate was obtained (flow rates are in Table 1). All other boundaries were treated as no-slip for the liquid phase and as free-slip for the gas.

The initial condition was set as follows. The liquid velocity was zero everywhere, the gas velocity was set to terminal bubble speed, and the gas volume fraction (voidage, holdup) e was set to $e = 0.001$ to help the solution to converge more easily at the beginning of the simulations. The gas started to flow into the column at time zero, $t = 0$. Then the real time interval of 60 s was simulated. After this period, the flow pattern with the liquid upflow in the centre and downflow near the walls of the column was developed. The results are shown in Fig. 4, as the voidage and velocity fields and radial profiles.

The voidage fields (Fig. 4a) show the typical voidage distribution in the case of a centrally sparged column, with the maximum holdup on the centreline and the depleted zones near the bottom. The highest holdup was found in the centre of the column, which also agrees with the literature (e.g. Shollenberger et al., 1997; Kumar et al., 1997; Parasu Veera and Joshi, 1999). The radial voidage profile turns flatter with increasing height, since the dispersive forces push the bubbles down the concentration gradient. Case B has lower voidage than Case D (ca. 1% vs. 4%), due to the lower gas input. The mean values of holdup obtained from the simulations (volume-average over the bubble column) corresponded to the experimentally determined values, both being of few percents (Cases A–D, simulation/experiment: 0.9/1, 0.9/1, 2.1/2, 4.2/4 in %). The radial holdup profiles (Fig. 4b) are rather insensitive to the liquid input (c.f. A and B), but are sensitive to the gas

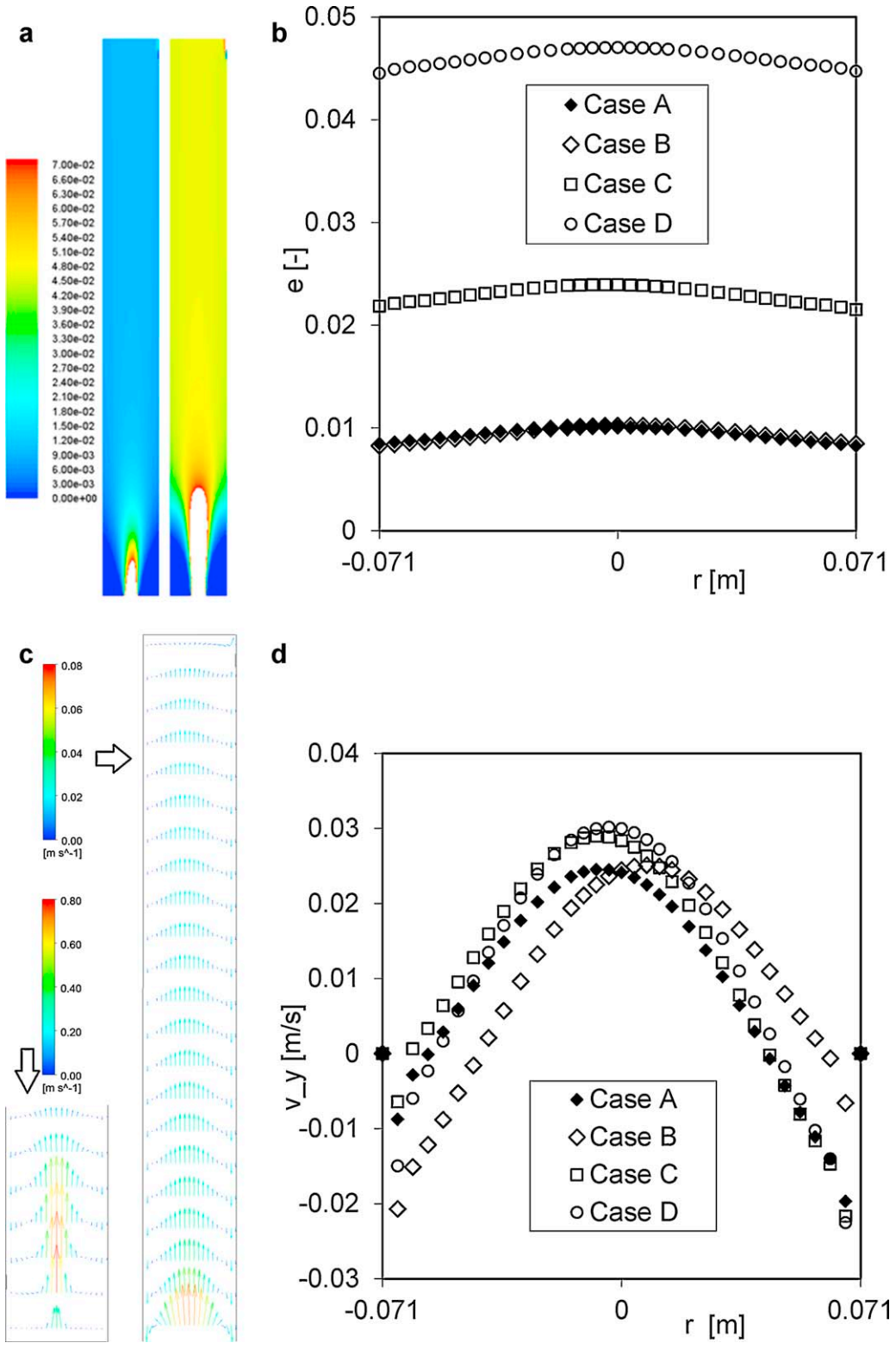

Fig. 4 – CFD simulation of the flow in the bubble column (Section 3.2). (a) Gas holdup field [–], Cases B and D. (b) Gas holdup radial profiles $e(r)$ at height $h = 0.7$ m, Cases A–D. (c) Liquid velocity field [m/s] in the domain symmetry plane, Case D. Left – high speed inlet region (1/4 of H). Right – low speed bulk region (3/4 of H). (d) Liquid velocity radial profiles $v_y(r)$ at height $h = 0.7$ m, Cases A–D.

input (c.f. B–D). While the mean holdups differ between the cases, the wall-axis holdup difference, which is the driving force for the liquid circulations, does not differ much. Consequently, the velocity profiles are expected to be similar. The liquid velocity field (Fig. 4c) shows the typical circulation-loop pattern, which is in agreement with the literature (e.g. Groen et al., 1996; Mudde et al., 1997; Jakobsen, 2001). The magnitude of the velocity vectors is highest at the gas distributor, comparable by order with the terminal bubble speed. The radial velocity profiles (Fig. 4d) are roughly parabolic and rather similar for all cases, with a relatively weak effect of the gas flow rate. The obtained flow field $\mathbf{V}(\mathbf{x})$ was further used for the calculation of the tracer transport within the bubble column (RTD) and for obtaining the fluid age field (SRTD).

Table 2 – Comparison of steady values of the mean residence time θ [s] of the liquid phase in the bubble column for Cases A–D obtained by different ways. Definition value is V/Q. Experimental values are obtained by the tracer pulse method (Section 4). RTD simulation values are from the numerical tracer experiment by CFD (Section 3.3). SRTD simulation values are from the age field computation by CFD (Section 3.4).

Case	Experiment	Simulation		
		V/Q	Classical RTD	SRTD
Case A	1816	1758	2012	1775
Case B	1029	999	1088	993
Case C	1077	986	1020	940
Case D	1084	966	1092	959

3.3. *RTD for bubble column – numerical results*

The tracer field in the liquid phase of the two-phase gas–liquid mixture was obtained by solving the multiphase analogue of the Eq. (1.2). Instead of the concentration (c), the tracer mass fraction (Y) in the liquid phase is used, $c = \rho Y/M$. The transport equation for the tracer then is

$$\frac{\partial(f\rho Y)}{\partial t} + \nabla\cdot(f\mathbf{V}\rho Y) = -\nabla\cdot(f\mathbf{J}), \quad \text{(RTD tracer equation)} \quad (3.3.1)$$

where f is the liquid volume fraction in the mixture ($e+f=1$), ρ is the liquid density, Y is the tracer mass fraction, $\mathbf{J}$ is the tracer diffusion flux, $\mathbf{J} = -(\rho D + \mu_t/\mathrm{Sc})\nabla Y$. The flux $\mathbf{J}$ consists of two parts, the molecular diffusion and the turbulent diffusion. The former is the standard gradient process in binary mixtures, with the tracer diffusivity D. The latter is the dispersing tendency of the flow, usually expressed in flow simulations with help of the turbulent viscosity μ_t and the Schmidt number Sc. The values of μ_t and Sc are given in Appendix A.

The single pulse of the tracer was applied in the form of the initial condition, where a small tracer amount were placed within a small volume (3 cm × 2 cm × 4 cm) of the liquid at the tracer entrance area at $h = 18$ cm, with $Y = 1$. After injecting the tracer, the period of 6 000 s of the flow time was simulated. Solving the two-phase flow equations (see Appendix A) and the tracer equation (1.2) gave the velocity fields of the gas $\mathbf{U}(\mathbf{x},t)$ and liquid $\mathbf{V}(\mathbf{x},t)$ phases and the tracer concentration field $c(\mathbf{x},t)$ in the liquid phase. The exit concentration averaged over the output cross-section area, $\hat{c}_e(t)$, was then obtained, whence the standard RTD function E, see Fig. 5. In the Case A, the E-curve is flatter and with its first momentum shifted to the right due to the lower liquid flow rate, as compared to the Case B, see Fig. 5a. The Cases B–D are close together, see Fig. 5b, since they have the same liquid input. Their difference in the gas input did not project much into the RTD data. The exit age obtained from the RTD tracer simulation is slightly higher the that calculated by definition as V/Q, where V is the liquid phase volume and Q is the liquid phase input, by 3–12%, see Table 2. This variance is mostly seen in the imperfectness of the multiphase CFD performance.

3.4. *SRTD for bubble column – numerical results*

The equation for the fluid age in a *single-phase* flow is given by Eq. (1.4). In engineering applications, the flow typically is not laminar and to calculate the complete velocity field $\mathbf{v}(\mathbf{x}, t)$ at all scales would be rather impractical. Therefore, we can decompose it into the mean and fluctuating parts, $\mathbf{v} = \mathbf{V} + \mathbf{v}'$.

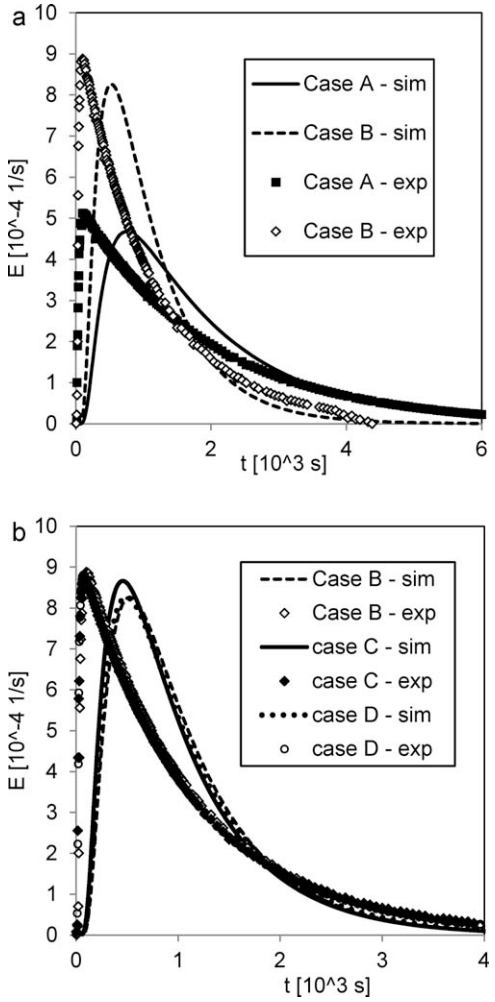

Fig. 5 – RTD in bubble column. CFD simulation (lines) vs. tracer experiment (marks). Distribution function $E(t)$ of the exit fluid age ($t = a$). (a) Cases A and B. (b) Cases B–D.

The mean part $\mathbf{V}$ can stay in the convective term, giving term $(\mathbf{V}\cdot\nabla)a$. The fluctuating part $\mathbf{v}'$ can be modelled with help of a dispersive mechanism, e.g. the turbulent dispersion, giving term $\nabla\cdot(D_T\nabla a)$. After this simplification, the Eq. (1.4) becomes

$$\left(\frac{\partial a}{\partial t}\right) + (\mathbf{V}\cdot\nabla)a = 1 + \nabla.(D_T\nabla a), \quad \text{(SRTD single-phase)} \quad (3.4.1)$$

where D_T is a suitable coefficient of the flow turbulent diffusivity (see Appendix A). The *multi-phase* version of Eq. (1.4) can be obtained with help of Eqs. (3.3.1) and (3.4.1). For our two-phase flow, namely for our liquid phase, the transport equation for the age a is suggested in the following form:

$$\frac{\partial(fa)}{\partial t} + \nabla\cdot(f\mathbf{V}a) = 1.\mathrm{f} + \nabla.(fD_T\nabla a). \quad \text{(SRTD multi-phase)} \quad (3.4.2)$$

Solving the two-phase flow equations (see Appendix A) and the fluid age equation (3.4.2) gives the velocity fields of the gas $\mathbf{U}(\mathbf{x}, t)$ and liquid $\mathbf{V}(\mathbf{x},t)$ phases, and the space-time distribution of the fluid age $a(\mathbf{x},t)$. The results are shown in Figs. 6–8. The spatio-temporal pattern of the liquid age $a = a(x,y;t)$ within the bubble column is shown in Fig. 6. The time evolution of the liquid age distribution is documented in a series of five different instants: 500, 1500, 3000, 4500 and 6000 s from the startup, for the Case B. The 'young' water of age $a = 0$ enters the column at the bottom-left and the 'old' water leaves it at the top-right, with the mean exit age of 460, 855, 975, 995 and 995 s,

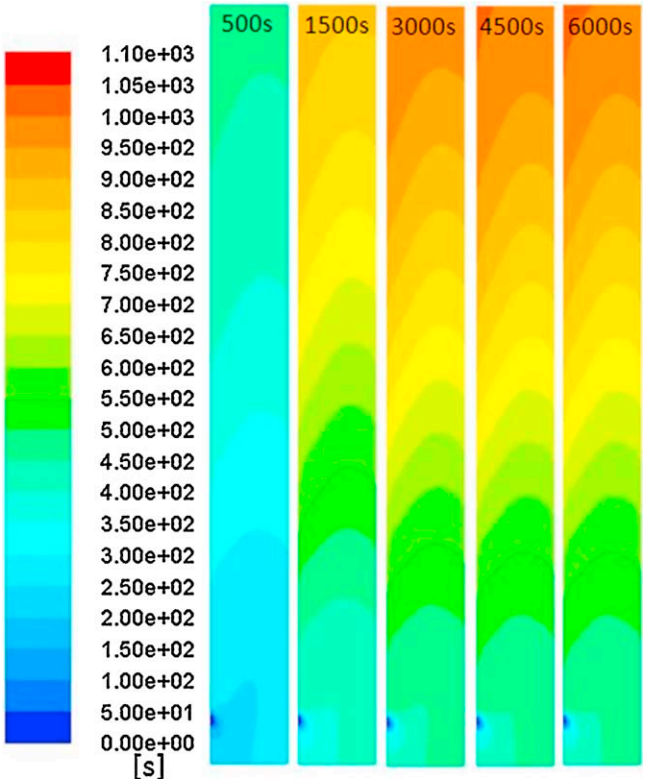

Fig. 6 – SRTD in bubble column. Patterns of the spatio-temporal dynamics of the liquid age distribution $a = a(x,y,t)$, in the domain symmetry plane for Case B. Time sequence of $t = 500$, 1500, 3000, 4500 and 6000 s.

respectively. The evolution of two important values of the fluid age are shown for Cases A and B in Fig. 7: (i) the mean value a_{in} taken over the flow domain interior, (ii) the mean value a_{ex} taken over the exit area. Obviously, the former should not be larger than the latter. For an ideal mixer, $a_{in} = a_{ex}$ and for a piston flow, $a_{in} = (1/2)a_{ex}$. In our case, the ratio $a_{in}/a_{ex} \approx 0.75$–0.8, which lies between these two limits. Case B has double liquid input than A (Table 1), whence it has lower inner and exit age (Fig. 7 and Table 2). The Cases B–D are of the same liquid input and also of similar age, Table 2. Note that the time course $a(t)$ of the fluid age in Fig. 7 can be obtained by SRTD but

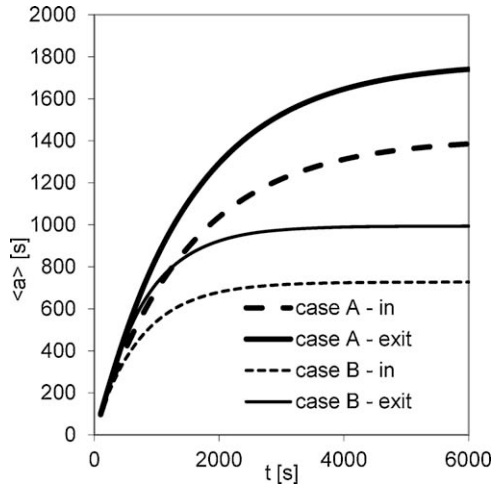

Fig. 7 – SRTD in bubble column. Evolution of the interior average fluid age a_{in} and the exit average fluid age a_{ex}. Cases A and B. The graphs curves tend to the steady values shown in Table 2.

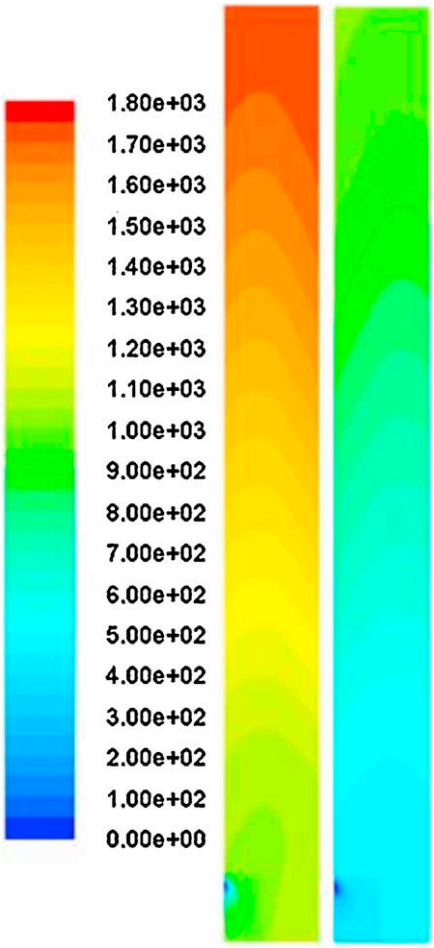

Fig. 8 – SRTD in bubble column. Effect of liquid input on the steady distribution of the fluid age in the symmetry plane. Case A of $Q_L = 44$ l/h and Case B of $Q_L = 80$ l/h (Table 1).

cannot be obtained by RTD. The shapes of these curves can be relevant for systems where transport and reaction phenomena occur, where biological agents is present, etc., because they indicate how fast the batch is 'aging'. Only the end points (steady values) can be obtained by RTD. The steady state spatial distribution $a(x,y)$ of the liquid age in the symmetry plane inside the bubble column for two Cases A and B is shown in Fig. 8. The age of system A is higher than of B, since the latter has roughly double liquid input than the former. The age is lowest near the liquid inlet and continuously increases to the top of the column, to the outlet. At the column cross-section, the age is higher near the walls and lower in the column centre, which corresponds to the liquid velocity profile. Note that Figs. 6 and 8 present unique information about the interior state of the contacting/reacting equipment, be it chemical or biological system. The structure of the age field $a(\mathbf{x},t)$ can easily indicate flow maldistribution and its consequences (substrate depletion, product accumulation, difference in reaction conversion, peaks of temperature or pressure, potentially unsafe locations, etc.). Nothing like this can be obtained by RTD.

4. Experiment on RTD in bubble column

4.1. *Experimental methods*

The experimental apparatus for the tracer RTD measurement was the cylindrical bubble column described in Section 3.1 (Fig. 3). The liquid phase RTD in the column was evaluated

from the response to the pulse injection of the tracer. The column was filled with tap water and the gas was let in. After a starting period no less than 15 min, the tracer was injected. The tracer was the NaCl salt, 200 g/l aqueous solution, of which 50 ml was injected manually with a syringe into the inlet pipe, at a distance of ca. 10 cm from the wall, within a short period of ca. 1 s.

The tracer concentration at the column exit was measured as the liquid phase conductivity. The conductivity meter used was BA51101/11.95/Pro/LF538-1, equipped with the conductivity probe TetraCon 325. The probe was calibrated in NaCl solutions and a linear correlation was obtained. The probe resolution was 0.01 μS/cm for the range <20 μS/cm and 0.1 μS/cm for 20 < 200 μS/cm. The peak values in our measurements were ~160 μS/cm. The conductivity data were recorded manually, read from the display. Typically, the conductivity was measured initially every 5 s for the first period of 120 s, then every 10 s until time of 1000s, and then every 30–60 s. The measurements were repeated 3-times and the graphs shown the mean over these three runs.

The voidage can be determined either from the pressure-difference along the column, or from the collapse of the bubble layer after switching-off the liquid in/out flows and the gas input.

4.2. *Experimental results vs. CFD simulations*

The tracer response curves *E*-curve measured in the experiments, for Cases A–D, are shown in Fig. 5. It can be seen, that there are only minor differences between the three curves corresponding to Cases B–D, which have the same liquid input. Therefore, within this range of the liquid input, the liquid velocity field responsible for the tracer transport is not much dependent on the gas input. This can be advantageously used in some applications, where we can vary the sparging within a certain range, but the flow pattern will not be affected much, whence the flow conditions for the bioprocess will be conserved. It is also seen from Fig. 5 that, the experimental system responds more quickly to the tracer pulse then the CFD simulations. This can be explained by the deficiencies of the Euler/Euler approach used in the CFD. The two-continua model cannot resolve the individual bubbles driving the liquid circulations upward in the centreline region of the column, at a speed comparable to the terminal bubble speed. Consequently, the rising liquid velocity is rather under-predicted in simulations. Besides, this approach cannot resolve the bubbles wakes and the liquid captured within them and their collective dynamics, also contributing to fast upward transport of the tracer. The CFD results are therefore plausible qualitatively, with a challenge for their further quantitative improvement.

5. Conclusions

The problem of the residence time distribution in the multiphase gas–liquid flow system (bubble column) was investigated with help of the two approaches. The first approach is the standard RTD, using the tracer techniques. The second denoted as Smart-RTD is based on a relatively new paradigm, which results in the actual spatio-temporal distribution of the fluid age $a(\mathbf{x},t)$ inside the apparatus. The following points have been reached:

- The relatively less known SRTD concept was highlighted to the chemical engineering community.
- The relation between the RTD and SRTD concepts was presented and discussed.
- The SRTD was formulated in case of multiphase flow systems.
- The spatio-temporal distribution of the liquid age was calculated for a bubble column by SRTD.
- The standard RTD was performed both by experiments and calculations.
- The obtained results on RTD and SRTD were compared and discussed.

To conclude, the SRTD concept originally developed for the ventilation problems in the field of the civil engineering presents a powerful tool also for chemical engineering. The direct knowledge of the fluid mean age distribution $a(\mathbf{x},t)$ within the interior space of our transport and reacting systems can highly be relevant for calculating the local efficiencies, indicating the localities of too low or high conversions, predicting potential hazards due to flow maldistributions. This equally holds also for bioengineering applications where SRTD shows places where the active biomass can be overloaded, suffers from the lack of substrate or oxygen, or is exposed to an adverse level of inhibitory products or toxins.

Acknowledgements

The financial support of GACR (Grant No. 104/07/1110), GA MSMT (No. LG11014) and from FCT (Fundacão para a Ciência e Tecnologia, SFRH/BD/37082/2007) is gratefully acknowledged.

Appendix A.

The Euler–Euler approach was used to model the gas–liquid flow in the bubble columns. The flow field is described by the continuity and momentum equations, for each phase, and have the following form (Fluent Inc., Fluent 12.1 Theory guide):

$$\frac{\partial(f\rho_L)}{\partial t} + \nabla\cdot(f\rho_L V) = 0 \quad (\text{mass } L) \tag{A1a}$$

$$\frac{\partial(e\rho_G)}{\partial t} + \nabla\cdot(e\,\rho_G\,U) = 0 \quad (\text{mass } G) \tag{A1b}$$

$$\frac{\partial(f\rho_L V)}{\partial t} + \nabla\cdot(f\rho_L VV) = -f\nabla p - \nabla\cdot(f\tau_L) + f\rho_L g + F_{LG}$$

(momentum L) (A2a)

$$\frac{\partial(e\rho_G U)}{\partial t} + \nabla\cdot(e\rho_G UU) = -e\nabla p - \nabla\cdot(e\tau_G) + e\rho_G g + F_{GL}$$

(momentum G) (A2b)

where e, f are the volume fractions of the gas and liquid phases. Here τ_L, τ_G are the effective stress tensors in the liquid and gas phases, with contributions from the viscous and turbulent effects,

$$\tau_L = \mu_{eff,L}(\nabla V + \nabla V^T) + \left(\kappa_L - \left(\frac{2}{3}\right)\mu_{eff,L}\right)\nabla\cdot VI,$$

(stress tensor L) (A3a)

$$\tau_G = \mu_{eff,G}(\nabla U + \nabla U^T) + \left(\kappa_G - \left(\frac{2}{3}\right)\mu_{eff,G}\right)\nabla \cdot UI,$$

(stress tensor G) (A3b)

where κ is the coefficient of bulk viscosity, I the identity matrix. The effective viscosity $\mu_{eff,q} = \mu_{l,q} + \mu_t$ is the sum of the molecular μ_l and turbulent μ_t viscosities. The former is a single-phase material parameter, while the latter depends on the flow. It can be expressed as

$$\mu_t = \frac{\rho_m C_\mu k^2}{\varepsilon}, \tag{A4}$$

and calculated by the standard (mixture) $k-\varepsilon$ model:

$$\begin{aligned}\frac{\partial(\rho_m k)}{\partial t} + \nabla\cdot(\rho_m V_m k) &= \nabla\cdot\left(\frac{\mu_t}{\sigma_k}\nabla k\right) + G_{k,m} - \rho_m\varepsilon\\ \frac{\partial(\rho_m \varepsilon)}{\partial t} + \nabla\cdot(\rho_m V_m \varepsilon) &= \nabla\cdot\frac{\mu_t}{\sigma_\varepsilon}\nabla\varepsilon + \frac{\varepsilon}{k}(C_{1,\varepsilon}G_{k,m} - C_{2,\varepsilon}\rho_m\varepsilon),\end{aligned} \tag{A5}$$

where ρ_m is mixture density, V_m is mass averaged velocity, $C_\mu = 0.09$, $C_{1,\varepsilon} = 1.44$, $C_{2,\varepsilon} = 1{,}92$, $\sigma_k = 1$, $\sigma_\varepsilon = 1.3$. $G_{k,m}$ is the production term of turbulent kinetic energy due to the shear. We considered two contributions to the interphase force, the drag and the turbulent dispersion,

$$F_{LG} = -F_{LG} = K(U-V) - KV_{dr}, \tag{A6}$$

where the first term is the drag and the second term is the turbulent dispersion. The drift velocity is

$$V_{dr} = -\left(\frac{D_{GPD}\nabla e}{\sigma_{GL} e} - \frac{D_{GPD}\nabla f}{\sigma_{GL} f}\right), \tag{A7}$$

where D_{GPD} is gas phase turbulent dispersivity and $\sigma_{GL} = 0.75$ is the turbulent Prandtl dispersion number. Further, it is:

$$\begin{aligned}K &= \left(\frac{3}{4}\right) ef\left(\frac{\rho_L}{d_p}\right) C_D|U-V|,\\ C_D &= \left(\frac{2}{3}\right)\left(\frac{d_p}{\lambda_{RT}}\right)\left[\frac{(1+17.67f*^{6/7})}{18.67f*}\right]^2,\end{aligned} \tag{A8}$$

where $\lambda_{RT} = [\sigma/(g\Delta\rho_{qp})]^{0.5}$, $f^* = (1-e)^{1.5}$. This gives the terminal bubble velocity in the limit of zero gas holdup equal to 23.1 cm/s for 5 mm equivalent diameter bubble (typical visually observed bubble size in our experiments). The surface tension was set to $0.073\,N\,m^{-1}$, liquid and gas density was 998.2 and $1.225\,kg/m^3$, respectively, liquid and gas viscosity was 0.001003 and $1.7894.10^{-5}\,kg\,m^{-1}\,s^{-1}$.

The dispersivity coefficient D_T in the tracer and fluid age equations contains contributions from the molecular diffusion and the turbulent diffusion. The former is the standard gradient process in binary mixtures, with tracer diffusivity D. The latter is the dispersing tendency of the flow (convection by flow structures, which are unresolved due to the use of a turbulent model). The value of D_T is expressed as

$$D_T = D + \frac{\nu_t}{Sc}. \tag{A9}$$

The solver default value was chosen for the turbulent Schmidt number $Sc = 0.7$. Kinematic turbulent viscosity $\nu_t = \mu_t/\rho_m$ is calculated from (A4). The tracer molecular diffusivity D was set to $2\times10^{-9}\,m^2/s^1$. In the case of fluid age transport equations the D was zero.

References

Andreux, R., Petit, G., Hemati, M., Simonin, O., 2008. Hydrodynamic and solid residence time distribution in a circulating fluidized bed: experimental and 3D computational study. Chemical Engineering and Processing 47, 463–473.

Baléo, J.N., Le Cloirec, P., 2000. Validating a prediction method of mean residence time spatial distributions. AIChE Journal 46, 675–683.

Baléo, J.N., Humeau, P., Le Cloirec, P., 2001. Numerical and experimental hydrodynamic studies of a lagoon pilot. Water Research 35, 2268–2276.

Claudel, S., Fonteix, C., Leclerc, J.P., Lintz, H.G., 2003. Application of the possibility theory to the compartment modelling of flow pattern in industrial processes. Chemical Engineering Science 58, 4005–4016.

Cockx, A., Do-Quang, Z., Line, A., Roustan, M., 1999. Use of computational fluid dynamics for simulating hydrodynamics and mass transfer in industrial ozonation towers. Chemical Engineering Science 54, 5085–5090.

Danckwerts, P.V., 1958. Local residence-times in continuous-flow systems. Chemical Engineering Science 9, 78–79.

Davidson, L., Olsson, E., 1987. Calculation of age and local purging flow rate in rooms. Building and Environment 22, 111–127.

Ekambara, K., Joshi, J.B., 2003. CFD simulation of residence time distribution and mixing in bubble column reactors. Canadian Journal of Chemical Engineering 81, 669–676.

Fluent Inc., Fluent 12.1 Theory Guide.

Froment, G.F., Bischoff, K.B., 1990. Chemical Reactor Analysis and Design.

Ghirelli, F., Leckner, B., 2004. Transport equation for the local residence time of a fluid. Chemical Engineering Science 59, 513–523.

Ghirelli, F., Hermansson, S., Thunman, H., Leckner, B., 2006. Reactor residence time analysis with CFD. Progress in Computational Fluid Dynamics 6, 241–247.

Groen, J.S., Oldeman, R.G.C., Mudde, R.F., van den Akker, H.E.A., 1996. Coherent structures and axial dispersion in bubble column reactors. Chemical Engineering Science 51, 2511–2520.

Hocine, S., Pibouleau, L., Azzaro-Pantel, C., Domenech, S., 2008. Modelling systems defined by RTD curves. Computers and Chemical Engineering 32, 3112–3120.

Jakobsen, H.A., 2001. Phase distribution phenomena in two-phase bubble column reactors. Chemical Engineering Science 56, 1049–1056.

Kumar, S.B., Moslemain, D., Dudukovic, M.P., 1997. Gas hold-up measurements in bubble columns using computed tomography. AIChE Journal 43, 1414–1425.

Le Moullec, Y., Potier, O., Gentric, C., Leclerc, J.P., 2008. Flowfield and residence time distribution simulation of a cross-flow gas–liquid wastewater treatment reactor using CFD. Chemical Engineering Science 63, 2436–2449.

Liu, M., Tilton, J.N., 2010. Spatial distributions of mean age and higher moments in steady continuous flows. AIChE Journal 56, 2561–2572.

Liu, M., 2011. A method for computing the degree of mixing in steady continuous flow systems. Chemical Engineering Science 63, 3045–3048.

Montastruc, L., Brienne, J.P., Nikov, I., 2009. Modeling of residence time distribution: application to a three-phase inverse fluidized bed based on a Mellin transform. Chemical Engineering Journal 148, 139–144.

Mudde, R.F., Groen, J.S., van den Akker, H.E.A., 1997. Liquid velocity field in a bubble column: LDA experiments. Chemical Engineering Science 52, 4217–4224.

Nauman, B.E., 2008. Residence time theory. Industrial & Engineering Chemistry Research 47, 3752–3766.

Parasu Veera, U., Joshi, J.B., 1999. Measurement of gas hold-up profiles by gamma ray tomography: effect of Sparger design

and height of dispersion in bubble columns. Chemical Engineering Research and Design 77, 303–317.
Pareek, V.K., Yap, Z., Brungs, M.P., Adesina, A.A., 2001. Particle residence time distribution (RTD) in three-phase annular bubble column reactor. Chemical Engineering Science 56, 6063–6071.
Prosperetti, A., Tryggvason, G., 2007. Computational Methods for Multiphase Flow. Cambridge University Press, New York.
Rafique, M., Chen, P., Dudukovic, M.P., 2004. Computational modeling of gas–liquid flow in bubble columns. Reviews in Chemical Engineering 20, 225–375.
Ranade, V.V., 2002. Computational Flow Modeling for Chemical Reactor Engineering. Academic Press.
Rigopoulos, S., Jones, A., 2003. A hybrid CFD—reaction engineering framework for multiphase reactor modelling: basic concept and application to bubble column reactors. Chemical Engineering Science 58, 3077–3089.
Ruzicka, M., 2008. On dimensionless numbers. Chemical Engineering Research and Design 86, 835–868.
Sandberg, M., 1981. What is ventilation efficiency? Building and Environment 16, 123–135.
Shollenberger, K.A., Torczyski, J.R., Adkins, D.R., O'Hern, T.J., Jackson, N.B., 1997. Gamma-densitometry tomography of gas hold-up spatial distribution in industrial bubble columns. Chemical Engineering Science 52, 2037–2048.
Spalding, D.B., 1958. A note on mean residence-times in steady flows of arbitrary complexity. Chemical Engineering Science 9, 74–77.